Structure and dynamics of dense colloidal ellipsoids at the nearest-neighbor length scale

Antara Pal,* Md. Arif Kamal, and Peter Holmqvist
Division of Physical Chemistry, Department of Chemistry, Lund University, Lund, Sweden

Peter Schurtenberger
Division of Physical Chemistry, Department of Chemistry, Lund University, Lund, Sweden and Lund Institute of Advanced Neutron and X-ray Science (LINXS), Lund, Sweden

(Received 23 February 2021; accepted 24 May 2021; published 29 June 2021)

Anisotropic particles are known to exhibit a richer and more complex phase behavior in comparison to their spherical counterpart. While the majority of the existing studies address structural properties, the dynamic behavior of anisotropic particles is a relatively lesser explored avenue. Using multispeckle ultra-small-angle x-ray photon correlation spectroscopy (USA-XPCS), we have carried out a systematic investigation of the structural and dynamic properties of colloidal ellipsoids at the nearest-neighbor length scale. The USA-XPCS measurements have allowed us to probe, as a function of the volume fraction, the q-dependent effective structure factor, $S_{\mathrm{eff}}(q)$, along with the effective long time diffusion coefficient, $D_{\mathrm{eff}}(q)$, for this anisotropic system. Our results indicate a scaling behavior of $D_{\mathrm{eff}}(q)$ with $1/S_{\mathrm{eff}}(q)$ from which we have estimated the effective amplitude function $A_{\mathrm{eff}}(q)$, which can be directly related to the effective hydrodynamic function $H_{\mathrm{eff}}(q)$. $A_{\mathrm{eff}}(q)$ shows a similar q dependence to that of $S(q)$. Our investigation also allows for the precise determination of the volume fraction corresponding to the arrest transition.

DOI: 10.1103/PhysRevResearch.3.023254

I. INTRODUCTION

Unlike their spherical counterparts, anisotropic particles exhibit a richer phase behavior with enhanced complexity due to their orientational degrees of freedom. In addition to the usual gas, liquid, crystal, and glass phases, anisotropic particles such as rods and plates are known to exhibit liquid crystalline phases [1,2]. While the majority of the existing studies address structural properties, not much is known about the dynamic behavior of anisotropic particles. The most well-studied systems in this regard are perhaps the colloidal rods and ellipsoids [3–7]. However, since most of these studies were carried out using the particle tracking method, they are all quasi-two-dimensional. Several studies combining polarized and depolarized light scattering have reported the average translational and rotational diffusion coefficients in the bulk [8–11] for different anisotropic particles. However, multiple scattering at high concentrations renders these measurements quite challenging, if not impossible. As a result, most of the studies have been carried out in the dilute regime, and barring a few reported cases, a systematic description of the dynamics near the ordered or arrested glassy phase is still lacking for bulk systems.

Theoretical studies on ellipsoidal particles predict a kinetic phase diagram as a function of packing fraction (ϕ) and aspect ratio (ρ) [12,13]. Three types of glass transitions have been predicted: the first is the conventional cage-driven one, which is typical for spherical particles, while the origins of the other two are related to the orientational degrees of freedom. For nonspherical particles, a glass phase is predicted that consists of nematic domains where the interdomain orientations build an orientational glass. Finally, a third type of glass transition is predicted for nearly spherical ellipsoids where the orientational degrees of freedom with odd-parity flips freeze independently from the positions.

Synchrotron-based multispeckle x-ray photon correlation spectroscopy (XPCS) using coherent x-rays has recently emerged as an alternative technique to study dynamics in diverse soft-matter systems such as colloids [14–17], polymers [18], gels [19–21], and supercooled liquids [22,23]. Although the basic principle of XPCS is analogous to that of dynamic light scattering (DLS), the use of x-rays instead of visible light makes it more suitable to circumvent problems related to multiple scattering and absorption that are often encountered in DLS when opaque systems made up of inorganic materials are investigated. Barring a few studies [14,24–26], the majority of the experimental studies reported in the literature that have used XPCS to study the dynamics of colloids have been predominantly restricted to the use of spherical particles [17,27,28]. The presence of anisotropy both in the particle shape as well as in their interaction potential will result in complex self-assembled structures and dynamics.

Herein, we present a detailed experimental study on the evolution of (an)isotropic dynamics of colloidal ellipsoids of $\rho = 2.9$ as a function of ϕ. Using XPCS in the ultra-small-angle regime, we have been able to investigate the dynamics at the nearest-neighbor length scale, d. At this length scale, XPCS probes the relaxation of the dominant local structure

*antara.pal@fkem1.lu.se

Published by the American Physical Society under the terms of the Creative Commons Attribution 4.0 International license. Further distribution of this work must maintain attribution to the author(s) and the published article's title, journal citation, and DOI.

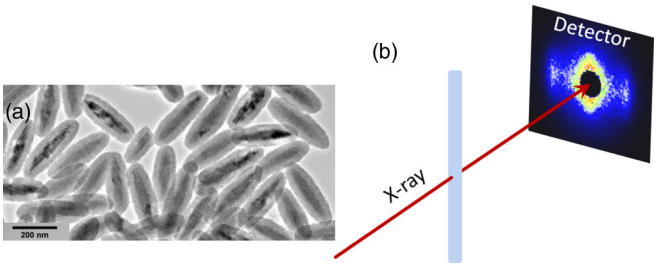

FIG. 1. (a) A representative TEM image of the core-shell hematite-silica colloidal ellipsoid. (b) Experimental scheme for the multispeckle ultra-small-angle x-ray photon correlation spectroscopy experiment.

determined by the nearest-neighbor cage. Our results indicate that at all the concentrations investigated, the density fluctuations relax via a single decay process, which can be related to the *long time* effective diffusion coefficient, D_{eff}. Further, D_{eff} scales as the *inverse* of the effective structure factor, $S_{\text{eff}}(q)$, for all ϕ. Analogous to the *effective hydrodynamic function*, $H_{\text{eff}}(q)$, which is the proportionality constant used in the scaling behavior of the effective *short time* diffusion coefficient, $D^s_{\text{eff}}(q)$, with the inverse of $S_{\text{eff}}(q)$ [29–34], we have defined the proportionality constant for the long time scaling behavior as an *effective amplitude function*, $A_{\text{eff}}(q)$. Using the aforementioned long time scaling, we have calculated $A_{\text{eff}}(q)$ for colloidal ellipsoids with $\rho = 2.9$, which shows a similar q dependence to that of $S_{\text{eff}}(q)$. We found that both the structural correlations and the diffusion coefficients are isotropic except at the highest concentration studied, $\phi_{\max} = 0.42$, where a nematic phase is formed. Further, the variation of D_{eff} as a function of ϕ indicates that the system approaches a kinetically arrested state at $\phi_m = 0.47$, which is in good agreement with the simulation.

II. EXPERIMENTAL SECTION

A. Synthesis

Hematite (Fe_2O_3) spindles were first synthesized in water following the approach described by Ocana *et al.* [35] and were later coated with a silica layer in ethanol using the method developed by Graf *et al.* [36]. After purification by repeated centrifugation/redispersion cycles in water, the colloidal particles were kept in water as a stock dispersion of 2.5 wt. %. Details of the synthesis of similar particles can be found elsewhere [37,38].

B. Characterization and methods

The characterization of the shape and size of the ellipsoidal colloids was carried out using transmission electron microscopy (TEM) (TEM-CM100 microscope from Phillips operating at 100 keV). From the resulting TEM images [Fig. 1(a)], using ImageJ, the particle size distribution was determined by analyzing at least 100 particles. The particle semilong (a) and semishort (b) axes were found to be $a = 156.7 \pm 12.2$ nm and $b = 53.7 \pm 4$ nm, respectively, leading to an aspect ratio of $\rho = 2.9$.

In view of their large size and high opacity, the dynamics of these particles was investigated using multispeckle ultra-small-angle x-ray photon correlation spectroscopy (USAXPCS). Experiments were performed at the beamline ID02, ESRF, in a pinhole ultra-small-angle x-ray scattering (USAXS) geometry. This unique instrument allows XPCS measurements on particle suspensions down to the μm^{-1} q-range [39]. A schematic of the experimental setup is shown in Fig. 1(b). The dispersion was filled in 1 mm capillaries, which were then flame-sealed in order to prevent the evaporation of water. In the next step, the individual capillaries were placed vertically such that the x-ray beam and the axis of the capillary are perpendicular to each other. Experiments were performed using an x-ray of wavelength 0.995 Å and a sample to detector distance of 20.0 m. The two-dimensional x-ray detection was achieved using a Eiger500K detector. The correlation functions were calculated using the PyXPCS software package, developed at beamline ID10, ESRF. For concentrations that show isotropic diffraction patterns ($0.17 \leqslant \phi < 0.42$), we have used an azimuthal average over 0 to 2π to extract information that depends only on the magnitude of q. However, since $\phi = 0.42$ shows an anisotropic diffraction pattern, we have used two different azimuthal sectors to analyze the data, as shown in Fig. 3(a).

III. RESULTS AND DISCUSSIONS

Both DLS and XPCS measurements provide information about the particle dynamics on a length scale which is of the order of $1/q$ via the intensity-intensity autocorrelation function,

$$g^{(2)}(\vec{q}, t) = \frac{\langle I(\vec{q}, \tau) I(\vec{q}, \tau + t)\rangle}{\langle I(\vec{q})\rangle^2}, \tag{1}$$

where $|\vec{q}| = 4\pi \sin(\theta/2)/\lambda$ is the magnitude of the scattering vector, θ is the scattering angle, and λ is the wavelength in the scattering medium. Figure 2 represents the structural correlation and dynamics at the lowest concentration, $\phi_{\min} = 0.17$. Concentrations lower than $\phi_{\min}$ could not be studied due to the inherent limitation in the speed of data acquisition set by the 2D detector. Figure 2(a) shows the scattering pattern which is in the form of a broad ring, indicating an isotropic arrangement of the particles with significant positional correlations. Figure 2(b) represents the effective structure factor, which is obtained by dividing $I(q)/\phi$ by the normalized intensity of a very dilute sample of concentration $\phi_{\text{dil}} = 0.0045$; here $I(q)$ is the radial intensity profile. The black symbols in Fig. 2(b) indicate the q values at which we have measured the dynamics of the system. Figure 2(c) shows the intensity autocorrelation functions, $g^{(2)}(q, t)$, of the sample for different q values. The intermediate scattering function $g^{(1)}(\vec{q}, t)$ is related to $g^{(2)}(\vec{q}, t)$ via the Siegert relation, $g^{(1)}(\vec{q}, t) = \sqrt{[g^{(2)}(\vec{q}, t) - 1]/\beta}$, where β is the coherence factor of the experimental setup. $g^{(1)}(q, t)$ can be described phenomenologically by a Kohlrausch-Williams-Watts (KWW) expression,

$$g^{(1)}(q, t) = \exp[-(t/t_c)^{\gamma}], \tag{2}$$

where t_c is the relaxation time and γ is the KWW exponent that depends on the mechanism responsible for the relaxation

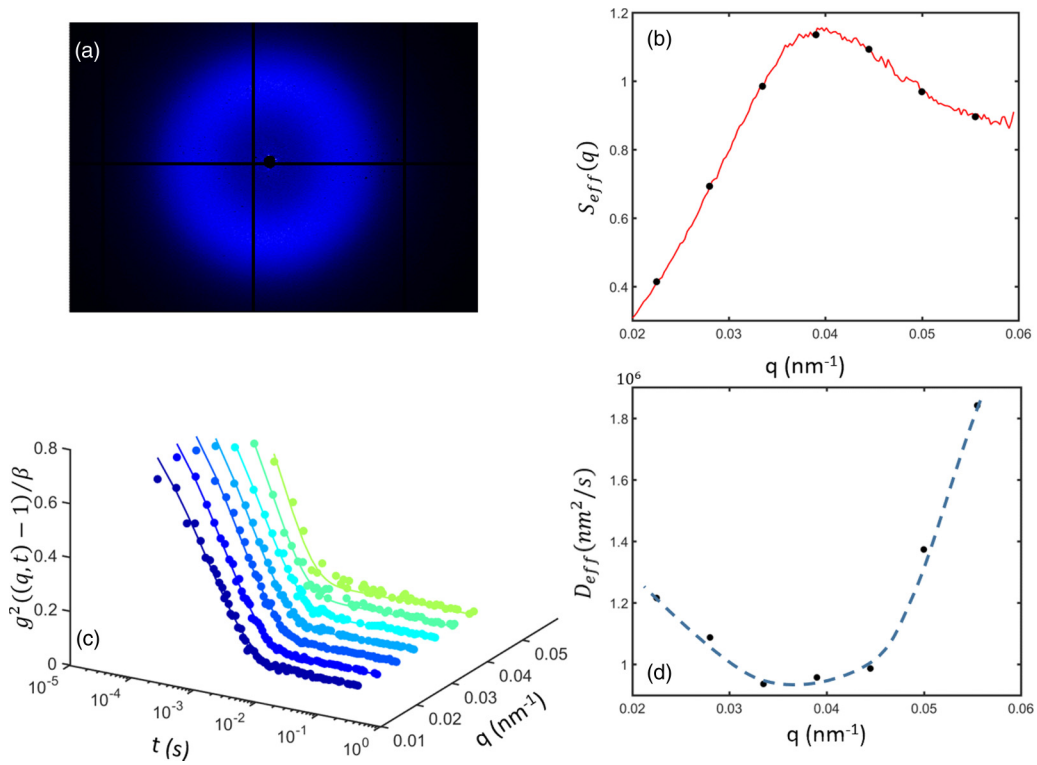

FIG. 2. (a) 2D scattering pattern and (b) effective structure factor for $\phi_{\min} = 0.17$. The black filled circles indicate the q values where the dynamics was measured. (c) Intensity autocorrelation functions for different q values indicated by the black filled circles in (b). The symbols represent the experimental data, while the line corresponds to the fit with the KWW model. (d) Variation of D_{eff} as a function of q; the black filled circles indicate the experimental data, and the blue dashed line is a guide to the eye.

of the density fluctuation. The average value of t_c is $\langle t_c \rangle = (t_c/\gamma)\Gamma(1/\gamma)$, where $\Gamma(1/\gamma)$ is the Euler Gamma function [40]. For freely diffusing (Brownian motion) particles, $\gamma = 1$ and $\langle t_c \rangle = t_c$. In this case, the relaxation time is related to the diffusion constant D by $1/\langle t_c \rangle = Dq^2$. In principle, for any value of γ we can still define an effective diffusion coefficient, $D_{\text{eff}} = 1/(\langle t_c \rangle q^2)$, which is shown in Fig. 2(d) as a function of q for $\phi_{\min}$. One can observe that $1/D_{\text{eff}}(q)$ follows a similar trend with q as $S_{\text{eff}}(q)$ [Fig. 2(b)]. This particular behavior, known as de Gennes narrowing, was initially described for simple liquids [41]. For colloidal short time diffusion, it can be mathematically represented as [29]

$$D^s_{\text{eff}}(q)/D_0 = H_{\text{eff}}(q)/S_{\text{eff}}(q), \tag{3}$$

where D_0 is the free-particle diffusion coefficient.

The relaxation of density fluctuation at the nearest-neighbor length scale exhibits increasingly separated short and long time processes that are qualitatively described by local diffusion or rattling in the nearest-neighbor cage, followed by the opening of the cage and subsequent diffusion out of the cage, respectively. At low volume fractions only a single relaxation process exists, while at higher volume fractions, once the interaction effects such as caging become strong enough, a separation between the short and long time diffusion emerges. The time scale (t) for short time diffusion is limited by $\tau_H \ll t \ll \tau_I$, where $\tau_H = R^2\rho_{\text{sol}}/\eta_{\text{sol}}\phi$ and $\tau_I = R^2/D_0$ [29]. Here, R is the particle radius, ρ_{sol} is the solvent density, and η_{sol} is the solvent viscosity. Given the size of our particles (50×150 nm), the limit of short time diffusion in our case comes out to be $10^{-9} \ll t \ll 10^{-2}$ s. As our measurements were performed within the time window $5 \times 10^{-5} \leqslant t \leqslant 10^{-1}$ s, our data are mainly dominated by the long time relaxation processes. For this system, we find that the variation of $1/D_{\text{eff}}(q)$ with q follows a trend that is similar to that followed by $S_{\text{eff}}(q)$ with q. Therefore, following Eq. (3), one can propose

$$D_{\text{eff}}(q)/D_0 = A_{\text{eff}}(q)/S_{\text{eff}}(q), \tag{4}$$

where $A_{\text{eff}}(q)$ is defined as the *effective amplitude function*. The majority of the studies in the literature have demonstrated that the short time diffusion coefficient follows $1/S_{\text{eff}}(q)$ behavior, whereas only a handful of them report about a similar scaling behavior for a long time diffusion coefficient [30,42,43] for both hard sphere and screened Coulomb interactions. Banchio *et al.* [43] have used simulations along with mode coupling theory and experiments to show the same scaling behavior for long time diffusion coefficients with $1/S_{\text{eff}}(q)$ as for short time ones. To the best of our knowledge, at present there is a lack of both theoretical and/or simulation studies that can account for this kind of scaling behavior for anisotropic particles. Interestingly, our experimental results clearly demonstrate that this phenomenological behavior also holds good for anisotropic systems as well.

Similar 2D scattering patterns indicating isotropic arrangement of particles have been observed for all concentrations except at $\phi_{\max} = 0.42$, where an anisotropic diffraction pattern representing the formation of a nematic phase is found.

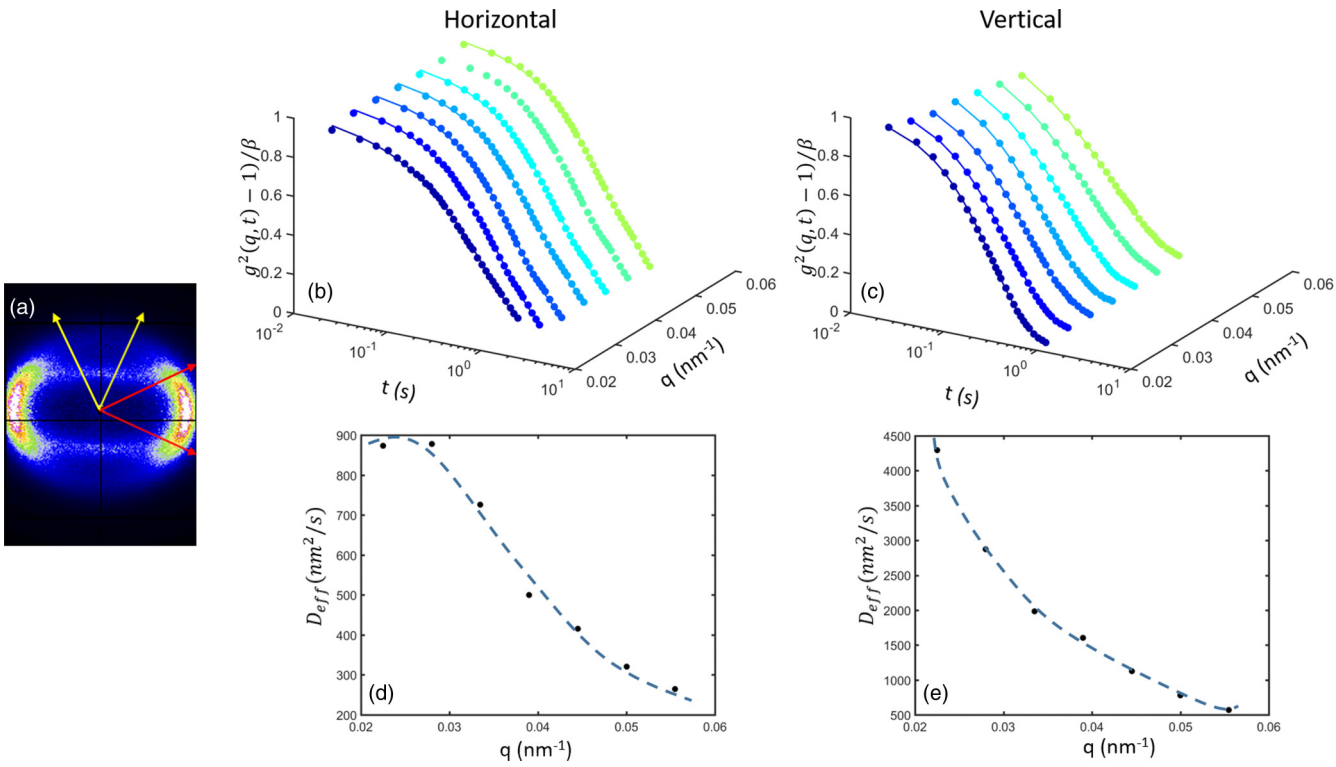

FIG. 3. (a) Experimentally measured 2D scattering pattern for $\phi_{max} = 0.42$. Azimuthal sector averages have been taken between two red (yellow) arrows to study the dynamics along the horizontal (vertical) direction. Intensity autocorrelation functions for different q values along (b) the horizontal and (c) the vertical direction, respectively. The symbols represent the experimental data while the line corresponds to the fit with the KWW model. Variation of $D_{eff}(q)$ as a function of q along (d) the horizontal and (e) the vertical direction, respectively; the black filled circles indicate the experimental data, and the blue dashed line is a guide to the eye.

The 2D diffraction pattern [Fig. 3(a)] at $\phi_{max} = 0.42$ exhibits a strong structural correlation along the horizontal direction. The structural peak along the horizontal direction corresponds to $q_{max} = 0.054$ nm^{-1}, indicating a nearest-neighbor distance of 116 nm, which is in reasonable agreement with the length of the short axes of the ellipsoids. To obtain the direction-dependent correlation functions, calculations were performed within two azimuthal sectors shown by red and yellow arrows [Fig. 3(a)], each defining a triangular region of interest along the horizontal and vertical direction, respectively. Comparing the intensity autocorrelation functions along horizontal and vertical directions, one can already see that along the horizontal direction, the relaxation time is slower than that along the vertical one [Figs. 3(b) and 3(c)]. The difference becomes quite prominent when one considers the variation of $D_{eff}(q)$ as a function of q as shown in Figs. 3(d) and 3(e); $D_{eff}(q)$ is almost three to five times larger along the vertical direction than the horizontal one depending on q. This anisotropy in $D_{eff}(q)$ is quite expected for a nematic phase where along the nematic periodicity particles are supposed to have lower mobility than that along the perpendicular direction.

Figures 4(a) and 4(b) represent the effective structure factor and the corresponding dynamics at different concentrations (represented by different colors), respectively. Since $\phi_{max} = 0.42$ shows an anisotropic diffraction pattern, in Fig. 4 we have used the data along the horizontal azimuthal sector [Fig. 3(a)]. As ϕ increases, the structural correlation builds up; the relative increase in the height of the structure factor peak accompanied by a decrease in its width with increasing ϕ [Fig. 4(a)] indicates an increase in the range of translational order. Further, the q value corresponding to the structure factor peak, q_m, shifts toward higher q with increasing ϕ, indicating a denser or closely packed system at higher concentration [Fig. 4(a) (inset)]. The shift of q_{max} with concentration follows a $\phi^{1/3}$ behavior (red continuous line), which is a characteristic of soft repulsive systems. Figure 4(b), which shows the variation of $1/D_{eff}(q)$ as a function of ϕ, indicates not only a de Gennes narrowing for the long time diffusion coefficient, but also a slowing down with increasing ϕ due to crowding effects or caging. Our findings are similar to those reported for spherical colloids [29–31], although the degree of structural correlation and the magnitude of the de Gennes narrowing is smaller for ellipsoids with comparable interaction potentials. Further, a strong jump in the dynamics can be seen at the highest concentration due to the onset of a phase transition to a nematic phase. In principle, having measured $S_{eff}(q)$ and $D_{eff}(q)$, one can now extract $A_{eff}(q)$ [by using Eq. (5)], shown in Fig. 4(c) for different concentrations. To calculate $A_{eff}(q)$, we have used $D_0 = 2.06 \times 10^6$ nm^2/s, measured using DLS at very dilute concentration, $\phi_{dil} = 0.0045$. One can see that $A_{eff}(q)$ also exhibits a strong q dependence and follows a trend similar to $S_{eff}(q)$. Further, if dynamic scaling is also valid for our ellipsoids with $A_{eff}(q)$ and $H_{eff}(q)$ being related by a multiplicative constant [30], then one can expect similar behavior for $H_{eff}(q)$ for this anisotropic system as well. Although there

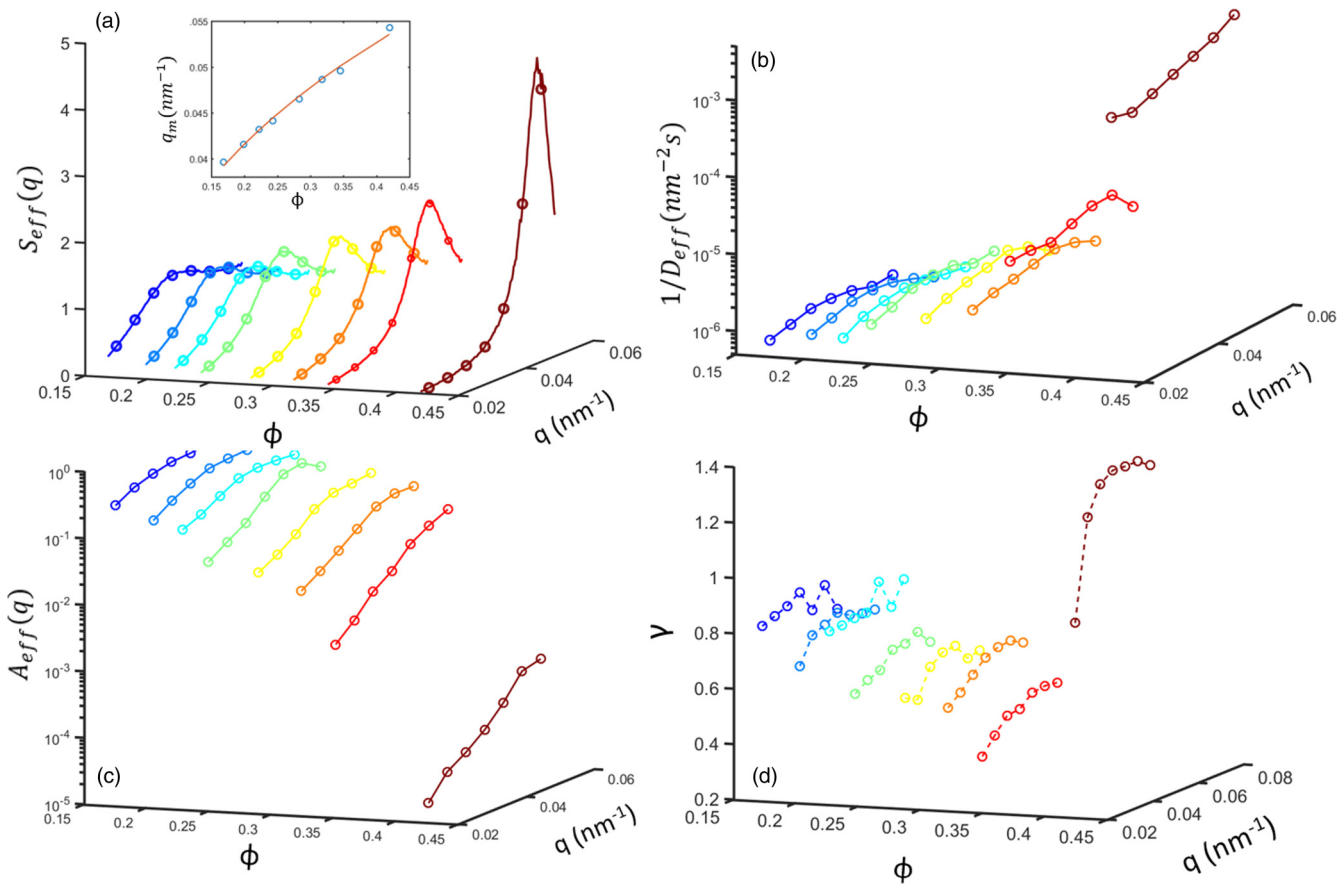

FIG. 4. (a) Variation of the structure factor $S_{\text{eff}}(q)$ as a function of q. The solid lines represent the experimental data, while the symbols indicate the q values where the dynamics was measured. The inset shows the variation of the q value corresponding to the structure factor peak, q_m, as a function of ϕ along with the fit with $q_m \propto \phi^{1/3}$ as a solid red line. (b) Variation of $1/D_{\text{eff}}(q)$ as a function of q. (c) Variation of the amplitude function $A_{\text{eff}}(q)$ as a function of q. (d) Variation of the exponent γ as a function of q. For (b), (c), and (d), the symbols indicate the experimental data while the solid lines are a guide to the eye. For all of (a), (b), (c), and (d), different colors correspond to different volume fractions ϕ.

are reports in the literature on the theoretical and experimental studies on $H_{\text{eff}}(q)$ for the hard and charged sphere systems [16,44,45], to the best of our knowledge there is no such experimental study on anisotropic particles.

From the fitting of the correlation functions, we observe that the stretching exponent, γ, in Eq. (2) changes with concentration. For ϕ_{min}, γ is just above 0.8, indicating a mild polydispersity or interaction-related contribution to the shape of the correlation functions. With an increase in concentration in the liquid regime, γ drops to a lower value ($\approx$0.5) at the highest concentration. Similar behavior has been reported in the literature for an anisotropic platelet system [11]. However, the situation changes drastically for ϕ_{max}, where the formation of a nematic phase is observed. For ϕ_{max}, the value of $\gamma > 1$ represents a compressed exponential behavior that may signify a hyperdiffusive process. This is expected for a highly ordered nematic phase, and it can be understood by considering the hopping of particles between the two nearest-neighbor sites. For a given value of q, γ decreases monotonically with increasing ϕ in the liquid phase followed by a sudden increase in the nematic phase (Fig. 5).

The concentration dependence of the normalized diffusion coefficient at q_m, $D_{\text{eff}}(q_m)/D_0$, can be seen in Fig. 6(a). When ϕ approaches the liquid-to-nematic phase transition, the diffusion coefficient is reduced strongly, almost four orders of

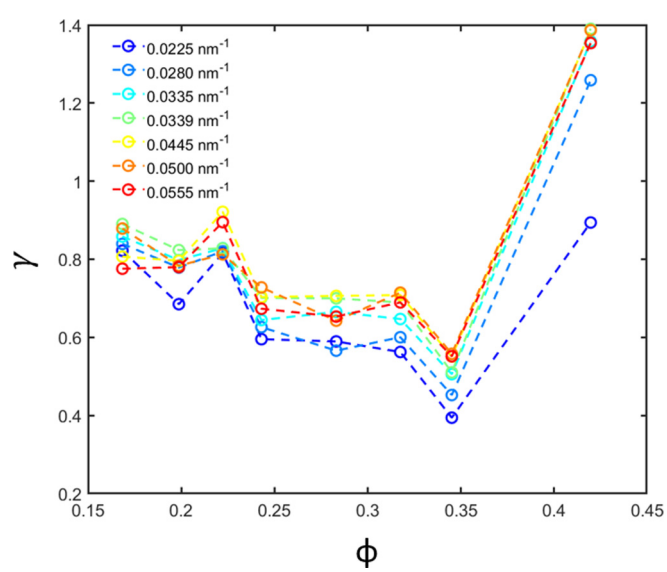

FIG. 5. Variation of γ as a function of ϕ for different q's.

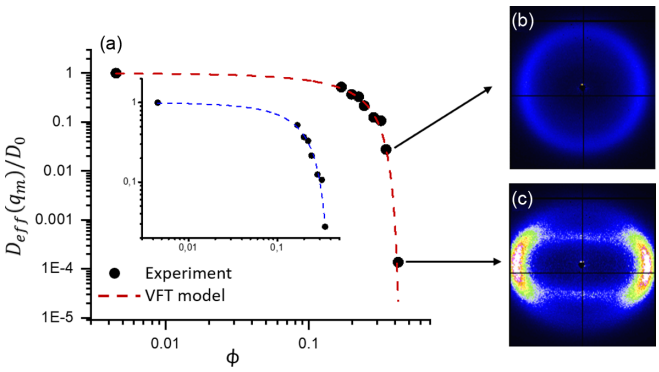

FIG. 6. (a) Variation of the normalized diffusion coefficient $D_{\text{eff}}(q_m)/D_0$ with ϕ; the symbols represent the experimental data, while the dashed line indicates the fit with modified VFT law. (b),(c) 2D scattering patterns for $\phi = 0.345$ (isotropic arrangement of particles) and $\phi = 0.42$ (formation of a nematic phase), respectively. The inset shows the fitting of the experimental data with VFT law excluding the data corresponding to ϕ_{max}.

magnitude compared to D_0. This clearly indicates that with an increase in ϕ, the system approaches kinetic arrest. We have fit our experimental data to the (modified) Vogel-Fulcher-Tammann (VFT) expression, which is usually used to describe the increase in viscosity of glass-forming molecular liquids with decreasing temperature. In the modified expression, temperature is replaced by $1/\phi$, because for colloidal dispersions ϕ plays a similar role to that of the temperature for molecular glasses. Further, for colloids, a modified VFT law is usually applied to describe the rise in the viscosity with ϕ and its dramatic increase at $\phi = \phi_m$ [46,47]. In our case, we have further modified it by replacing η_{sol}/η_0, where η_{sol} and η_0 are the viscosity of the solvent and the zero shear viscosity of the system, respectively, with $D_{\text{eff}}(q_m)/D_0$, to obtain a mathematical expression:

$$D_{\text{eff}}(q_m)/D_0 = \exp\left(\frac{F\phi}{\phi_m - \phi}\right). \tag{5}$$

The fit of Eq. (5) can be seen in Fig. 6(a) as the dashed line, where we found ϕ_m to be 0.47.

The system thus shows an isotropic arrangement of particles until $\phi = 0.345$ [Fig. 6(b)], and at $\phi = \phi_{\text{max}} = 0.42$ the formation of a nematic phase is observed, as is evident from the diffraction pattern shown in Fig. 6(c). This indicates that the isotropic to nematic transition lies between $\phi = 0.34$ and 0.42, which is in good agreement with the phase diagram predicted by simulation [48]. However, the data shown in Fig. 6(a) also indicate that while the slowing down of long time collective diffusion and dynamical arrest is due to the formation of nearest-neighbor cages, the arrest occurs within the nematic phase, while the simulations suggest that for $\rho \geqslant 2$, the slowing down mechanism is driven by a precursor of nematic order [13]. Given this discrepancy, we obviously need to test whether the resulting fit with Eq. (5) shown in Fig. 6(a) is strongly biased by the data point that lies in the nematic phase. Therefore, we have also fitted our experimental data with Eq. (5), but excluding the data for ϕ_{max} shown in Fig. 6 (inset), resulting again in a value $\phi_m = 0.47$.

Unfortunately, there are only a few studies available in the literature regarding the structural and dynamic properties of ellipsoidal colloids with comparable axial ratios in the vicinity of the arrest transition [49–51]. One of them describes dynamical arrest based on rheological measurements [51] for ellipsoidal particles with an axial ratio $\rho = 4.8$ without providing information on the structure and dynamics of the system. The other two describe the glass transition in bulk ellipsoidal systems with insight into the underlying arrest scenario based on a characterization of either collective or self-diffusion and complementary structural information from DDM ($\rho = 3.76$ [49]) or confocal microscopy ($\rho = 3.5$ [50]). Both studies find no evidence for a bulk nematic phase prior to dynamical arrest, quite in contrast to our observations. Although the actual particle systems and their axial ratios used in the different investigations were not identical, this discrepancy nevertheless raises questions. While the difference between the simulation results [13] and our experimental observations could possibly be accounted for by considering a soft repulsive potential from weakly screened residual charges and polydispersity in our system, this seems an unlikely explanation for the different findings in the other experimental studies given the similarity in polydispersity and surface characteristics for the particles used in at least one of these other studies [49]. One possibility could be that the suspensions are subjected to sufficiently large shear forces when filling them into the capillaries. This could lead to a shear-induced alignment of prenematic domains, resulting in a measurable bulk anisotropy, indicating the formation of a nematic phase. It is clear that further investigations into the phase behavior and dynamical arrest of ellipsoidal particles are needed to shed more light on the collective dynamics and the origin of dynamical arrest in these systems.

IV. CONCLUSION

In this article, we report the dynamics of colloidal ellipsoids at the nearest-neighbor length scale over a broad concentration range by employing ultra-small-angle XPCS. Although the literature is replete with simulations investigating the glass transition for ellipsoidal particles, there is a scarcity of experimental reports on these systems. It is for this reason that we have performed a systematic study of the structural and dynamical properties of a model ellipsoid system using XPCS. With this study, we have not only shown the relation between the self-assembled structure and dynamics, but we also determined experimentally the amplitude function for an anisotropic system. Although there are several reports in the literature pertaining to the scaling behavior of the short time diffusion coefficient with the inverse of the effective structure factor for (an)isotropic systems, to the best of our knowledge our study is the first one to shows that an analogous scaling behavior also exists for the long time diffusion coefficient for an anisotropic system. There remain, however, a number of questions when comparing our current findings with those previously reported for other, similar systems. Additional studies are clearly needed, in particular aiming at information about the rotational dynamics and short-time collective diffusion on nearest-neighbor length scales when approaching dynamical arrest. While such

information could in principle also be obtained from XPCS, it will require significant improvement in the time resolution of two-dimensional XPCS detectors required for such studies. Moreover, a quantitative understanding of our findings for the q-dependent long-time collective diffusion coefficient will also require further simulations that include an appropriate treatment of hydrodynamic interactions.

Until recently, measuring the collective dynamics of anisotropic colloidal particles at the nearest-neighbor length scale at these high concentrations would have been perceived as very difficult experimentally. The traditional experimental tools such as DLS or confocal microscopy require transparent systems, and there is a lack of available model systems that are suitable for high concentration studies. However, our investigation has demonstrated that XPCS allows us to circumvent this problem and characterize different anisotropic systems as they undergo a colloidal glass transition. This opens up new avenues for exploring the dynamics of strongly interacting colloidal systems with a large variety of shapes and chemical compositions. We believe that our results will inspire future experimental studies on concentrated anisotropic particles.

ACKNOWLEDGMENTS

T. Narayanan and T. Zinn are acknowledged for their help during XPCS measurements. T. Ito is acknowledged for help during synthesis. Crispin Hetherington is acknowledged for TEM measurement. Financial support from the European Research Council (Grant No. ERC-339678-COMPASS) and the Knut and Alice Wallenberg Foundation (Project Grant No. KAW 2014.0052) is gratefully acknowledged. ESRF is acknowledged for granting the beamtime.

[1] G. J. Vroege and H. N. Lekkerkerker, Phase transitions in lyotropic colloidal and polymer liquid crystals, Rep. Prog. Phys. **55**, 1241 (1992).

[2] H. Lekkerkerker and G. Vroege, Liquid crystal phase transitions in suspensions of mineral colloids: New life from old roots, Phil. Trans. R. Soc. A **371**, 20120263 (2013).

[3] C. K. Mishra, A. Rangarajan, and R. Ganapathy, Two-Step Glass Transition Induced by Attractive Interactions in Quasi-Two-Dimensional Suspensions of Ellipsoidal Particles, Phys. Rev. Lett. **110**, 188301 (2013).

[4] Z. Zheng, R. Ni, F. Wang, M. Dijkstra, Y. Wang, and Y. Han, Structural signatures of dynamic heterogeneities in monolayers of colloidal ellipsoids, Nat. Commun. **5**, 3829 (2014).

[5] Z. Zheng and Y. Han, Self-diffusion in two-dimensional hard ellipsoid suspensions, J. Chem. Phys. **133**, 124509 (2010).

[6] Z. Zheng, F. Wang, Y. Han *et al.*, Glass Transitions in Quasi-Two-Dimensional Suspensions of Colloidal Ellipsoids, Phys. Rev. Lett. **107**, 065702 (2011).

[7] M. J. Solomon and P. T. Spicer, Microstructural regimes of colloidal rod suspensions, gels, and glasses, Soft Matter **6**, 1391 (2010).

[8] D. Lehner, H. Lindner, and O. Glatter, Determination of the translational and rotational diffusion coefficients of rodlike particles using depolarized dynamic light scattering, Langmuir **16**, 1689 (2000).

[9] J. Rodríguez-Fernández, J. Pérez-Juste, L. M. Liz-Marzán, and P. R. Lang, Dynamic light scattering of short au rods with low aspect ratios, J. Phys. Chem. C **111**, 5020 (2007).

[10] I. Martchenko, H. Dietsch, C. Moitzi, and P. Schurtenberger, Hydrodynamic properties of magnetic nanoparticles with tunable shape anisotropy: Prediction and experimental verification, J. Phys. Chem. B **115**, 14838 (2011).

[11] D. Kleshchanok, M. Heinen, G. Nägele, and P. Holmqvist, Dynamics of charged gibbsite platelets in the isotropic phase, Soft Matter **8**, 1584 (2012).

[12] R. Schilling and T. Scheidsteger, Mode coupling approach to the ideal glass transition of molecular liquids: Linear molecules, Phys. Rev. E **56**, 2932 (1997).

[13] M. Letz, R. Schilling, and A. Latz, Ideal glass transitions for hard ellipsoids, Phys. Rev. E **62**, 5173 (2000).

[14] A. Pal, T. Zinn, M. A. Kamal, T. Narayanan, and P. Schurtenberger, Anomalous dynamics of magnetic anisotropic colloids studied by XPCS, Small **14**, 1802233 (2018).

[15] A. Pal, M. A. Kamal, T. Zinn, J. K. G. Dhont, and P. Schurtenberger, Anisotropic dynamics of magnetic colloidal cubes studied by x-ray photon correlation spectroscopy, Phys. Rev. Materials **5**, 035603 (2021).

[16] A. J. Banchio, J. Gapinski, A. Patkowski, W. Häußler, A. Fluerasu, S. Sacanna, P. Holmqvist, G. Meier, M. P. Lettinga, and G. Nägele, Many-Body Hydrodynamic Interactions in Charge-Stabilized Suspensions, Phys. Rev. Lett. **96**, 138303 (2006).

[17] A. Robert, E. Wandersman, E. Dubois, V. Dupuis, and R. Perzynski, Glassy dynamics and aging in a dense ferrofluid, Europhys. Lett. **75**, 764 (2006).

[18] K. L. Brinker, S. G. Mochrie, and W. R. Burghardt, Equilibrium dynamics of a polymer bicontinuous microemulsion, Macromolecules **40**, 5150 (2007).

[19] A. Papagiannopoulos, T. Waigh, A. Fluerasu, C. Fernyhough, and A. Madsen, Microrheology of polymeric solutions using x-ray photon correlation spectroscopy, J. Phys.: Condens. Matter **17**, L279 (2005).

[20] V. Trappe, E. Pitard, L. Ramos, A. Robert, H. Bissig, and L. Cipelletti, Investigation of q-dependent dynamical heterogeneity in a colloidal gel by x-ray photon correlation spectroscopy, Phys. Rev. E **76**, 051404 (2007).

[21] A. Fluerasu, A. Moussaïd, A. Madsen, and A. Schofield, Slow dynamics and aging in colloidal gels studied by x-ray photon correlation spectroscopy, Phys. Rev. E **76**, 010401(R) (2007).

[22] C. Caronna, Y. Chushkin, A. Madsen, and A. Cupane, Dynamics of Nanoparticles in a Supercooled Liquid, Phys. Rev. Lett. **100**, 055702 (2008).

[23] H. Guo, G. Bourret, M. K. Corbierre, S. Rucareanu, R. B. Lennox, K. Laaziri, L. Piche, M. Sutton, J. L. Harden, and R. L. Leheny, Nanoparticle Motion within Glassy Polymer Melts, Phys. Rev. Lett. **102**, 075702 (2009).

[24] A. Schavkan, *Dynamics of colloidal systems of magnetic nanoparticles under influence of magnetic fields investigated by XPCS*, DESY thesis, Deutsches Elektronen-Synchrotron DESY (2017).

[25] T. Hoshino, M. Nakayama, S. Fujinami, T. Nakatani, Y. Kohmura, and T. Kato, Static structure and dynamical behavior of colloidal liquid crystals consisting of hydroxyapatite-based nanorod hybrids, Soft Matter **15**, 3315 (2019).

[26] P. Holmqvist, V. Meester, F. Westermeier, and D. Kleshchanok, Rotational diffusion in concentrated platelet systems measured with x-ray photon correlation spectroscopy, J. Chem. Phys. **139**, 084905 (2013).

[27] E. Wandersman, Y. Chushkin, E. Dubois, V. Dupuis, A. Robert, and R. Perzynski, Field induced anisotropic cooperativity in a magnetic colloidal glass, Soft Matter **11**, 7165 (2015).

[28] F. Dallari, A. Martinelli, F. Caporaletti, M. Sprung, G. Grübel, and G. Monaco, Microscopic pathways for stress relaxation in repulsive colloidal glasses, Sci. Adv. **6**, eaaz2982 (2020).

[29] A. J. Banchio and G. Nägele, Short-time transport properties in dense suspensions: From neutral to charge-stabilized colloidal spheres, J. Chem. Phys. **128**, 104903 (2008).

[30] P. N. Segre and P. N. Pusey, Scaling of the Dynamic Scattering Function of Concentrated Colloidal Suspensions, Phys. Rev. Lett. **77**, 771 (1996).

[31] W. Van Megen, R. Ottewill, S. Owens, and P. N. Pusey, Measurement of the wave-vector dependent diffusion coefficient in concentrated particle dispersions, J. Chem. Phys. **82**, 508 (1985).

[32] B. M. Fine, A. Lomakin, O. O. Ogun, and G. B. Benedek, Static structure factor and collective diffusion of globular proteins in concentrated aqueous solution, J. Chem. Phys. **104**, 326 (1996).

[33] M. Adam and M. Delsanti, Dynamical properties of polymer solutions in good solvent by rayleigh scattering experiments, Macromolecules **10**, 1229 (1977).

[34] U. Zettl, S. T. Hoffmann, F. Koberling, G. Krausch, J. Enderlein, L. Harnau, and M. Ballauff, Self-diffusion and cooperative diffusion in semidilute polymer solutions as measured by fluorescence correlation spectroscopy, Macromolecules **42**, 9537 (2009).

[35] M. Ocaña, M. Morales, and C. Serna, Homogeneous precipitation of uniform α-fe 2 o 3 particles from iron salts solutions in the presence of urea, J. Colloid Interface Sci. **212**, 317 (1999).

[36] C. Graf, D. L. Vossen, A. Imhof, and A. van Blaaderen, A general method to coat colloidal particles with silica, Langmuir **19**, 6693 (2003).

[37] M. Reufer, H. Dietsch, U. Gasser, A. Hirt, A. Menzel, and P. Schurtenberger, Morphology and orientational behavior of silica-coated spindle-type hematite particles in a magnetic field probed by small-angle x-ray scattering, J. Phys. Chem. B **114**, 4763 (2010).

[38] I. Martchenko, J. J. Crassous, A. M. Mihut, E. Bialik, A. M. Hirt, C. Rufier, A. Menzel, H. Dietsch, P. Linse, and P. Schurtenberger, Anisotropic magnetic particles in a magnetic field, Soft Matter **12**, 8755 (2016).

[39] T. Zinn, A. Homs, L. Sharpnack, G. Tinti, E. Fröjdh, P.-A. Douissard, M. Kocsis, J. Möller, Y. Chushkin, and T. Narayanan, Ultra-small-angle x-ray photon correlation spectroscopy using the eiger detector, J. Synch. Radiat. **25**, 1753 (2018).

[40] C. Lindsey and G. Patterson, Detailed comparison of the williams-watts and cole-davidson functions, J. Chem. Phys. **73**, 3348 (1980).

[41] P. G. De Gennes, Liquid dynamics and inelastic scattering of neutrons, Physica **25**, 825 (1959).

[42] P. Holmqvist and G. Nägele, Long-Time Dynamics of Concentrated Charge-Stabilized Colloids, Phys. Rev. Lett. **104**, 058301 (2010).

[43] A. J. Banchio, M. Heinen, P. Holmqvist, and G. Nägele, Short- and long-time diffusion and dynamic scaling in suspensions of charged colloidal particles, J. Chem. Phys. **148**, 134902 (2018).

[44] J. Riest, T. Eckert, W. Richtering, and G. Nägele, Dynamics of suspensions of hydrodynamically structured particles: Analytic theory and applications to experiments, Soft Matter **11**, 2821 (2015).

[45] J. Gapinski, A. Patkowski, A. Banchio, J. Buitenhuis, P. Holmqvist, M. Lettinga, G. Meier, and G. Nägele, Structure and short-time dynamics in suspensions of charged silica spheres in the entire fluid regime, J. Chem. Phys. **130**, 084503 (2009).

[46] G. Brambilla, D. El Masri, M. Pierno, L. Berthier, L. Cipelletti, G. Petekidis, and A. B. Schofield, Probing the Equilibrium Dynamics of Colloidal Hard Spheres Above the Mode-Coupling Glass Transition, Phys. Rev. Lett. **102**, 085703 (2009).

[47] J. Mattsson, H. M. Wyss, A. Fernandez-Nieves, K. Miyazaki, Z. Hu, D. R. Reichman, and D. A. Weitz, Soft colloids make strong glasses, Nature **462**, 83 (2009).

[48] C. De Michele, R. Schilling, and F. Sciortino, Dynamics of Uniaxial Hard Ellipsoids, Phys. Rev. Lett. **98**, 265702 (2007).

[49] A. Pal, V. A. Martinez, T. H. Ito, J. Arlt, J. J. Crassous, W. C. Poon, and P. Schurtenberger, Anisotropic dynamics and kinetic arrest of dense colloidal ellipsoids in the presence of an external field studied by differential dynamic microscopy, Sci. Adv. **6**, eaaw9733 (2020).

[50] J. Roller, A. Laganapan, J.-M. Meijer, M. Fuchs, and A. Zumbusch, Observation of liquid glass in suspensions of ellipsoidal colloids, Proc. Natl. Acad. Sci. (USA) **118**, e2018072118 (2021).

[51] M. Solomon and D. Boger, The rheology of aqueous dispersions of spindle-type colloidal hematite rods, J. Rheol. **42**, 929 (1998).